THE JOURNAL OF PHYSICAL CHEMISTRY A
A JOURNAL OF THE AMERICAN CHEMICAL SOCIETY

pubs.acs.org/JPCA

Article

Theoretical Study of the Isotope Effect in Optical Rotation

Brian Faintich, Taylor Parsons, Ty Balduf, and Marco Caricato*

Cite This: J. Phys. Chem. A 2024, 128, 8045−8059

Read Online

ACCESS | Metrics & More | Article Recommendations | Supporting Information

ABSTRACT: In this work, the isotope effect in optical rotation (OR) is examined by exploring structure−property relationships for H → D substitutions in chiral molecules. While electronic effects serve as the dominant source of optical activity, there is a non-negligible contribution from nuclear vibrations, which changes with isotopic substitution. We employ a test set of 50 small organic molecules: three-membered rings with varying heteroatoms (PCl, PH, S, NCl, NH, O, and NBr) and functional groups (Me, F), and simulations were run at the B3LYP/aug-cc-pVDZ level of theory. The objectives of this work are to determine locations of isotopic substitution that result in significant changes in the vibrational correction to the OR and to evaluate which vibrational modes and electronic response are the major contributors to the isotope effect. Molecules with more polarizable heteroatoms in the ring (e.g., S and P) have the largest change in the vibrational correction compared to the unsubstituted parent molecules. In many cases, isotopic substitution made to the hydrogens on the opposite side of the ring from the functional group provides the largest change in the OR. H/D wagging modes and C vibrations (for D-C centers) are the largest contributors to the isotope effect. This is explained with a molecular orbital decomposition analysis of the OR. The relevant vibrational modes affect the orbital transitions that are already significant at the equilibrium geometry. However, this effect is only large when polarizable heteroatoms are involved because the electron density surrounding them is diffuse enough to feel the subtle effect of change in mass due to isotopic substitution on the relevant vibrational modes.

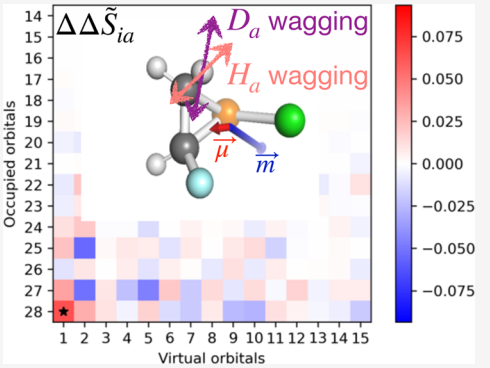

1. INTRODUCTION

Chiral molecules have nonsuperimposable mirror images, known as enantiomers, which are indistinguishable in achiral environments.[1,2] Although chiral molecules have the same physical properties, such as solubility and melting point, they behave differently in chiral environments such as the human body.[3−5] Therefore, the ability to distinguish between enantiomers is paramount in biological contexts and in the production of drugs. Nondestructive differentiation can be done using chiral light.[6−8] One of these chiroptical techniques is the measurement of optical rotation (OR), which occurs when plane-polarized light passes through a chiral sample and the plane of polarization is rotated. Quantum mechanical simulations have been extensively used to compare with experiments and to determine the absolute configuration of chiral samples.[9−25] Although the OR can be measured experimentally and calculated theoretically, structure−property relationships are still not well understood. In this work, we investigate one aspect of these relationships: the isotope effect on optical rotation through H → D substitutions.

Isotopic substitution has well-known effects on molecular properties. Probably the most direct effect is the change in the frequency of vibrational stretching through the change in the reduced mass of the vibrational mode. As a consequence, a deuterium-containing molecule will have a lower zero-point energy compared to the parent compound with hydrogen. Another example of the isotope effect is in kinetics, where there is a higher enthalpy of activation for reactions involving D instead of H.[26] The isotope effect has been also investigated in chirality, mostly on electronic and especially vibrational circular dichroism (ECD and VCD) spectra.[27−32] In terms of optical rotation, the observed effect on typical organic chiral molecules so far has been small[31] and it has not received much theoretical attention beyond some early models.[33] Note that the effect on the OR is purely vibrational, as isotopic substitution does not directly affect the electronic wave function within the Born−Oppenheimer approximation. In the case of self-assembly of chiral molecules, it was observed that isotopic substitution favors the formation of helical structures of a particular handedness.[34,35] This is due to a slight energy bias in the interaction energy between monomers in a specific conformation.[34] However, these studies do not present a systematic investigation of the nature of the isotope effect on the optical rotation.

Received: June 4, 2024
Revised: September 3, 2024
Accepted: September 4, 2024
Published: September 11, 2024

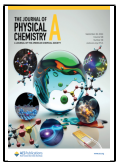

https://doi.org/10.1021/acs.jpca.4c03728
J. Phys. Chem. A 2024, 128, 8045−8059

The objective of this work is to determine how isotopic substitution affects the OR in chiral molecules and which locations of the substitution maximize the effect. While the electronic effects are the dominant contribution to the OR, the vibrational correction is in general a non-negligible contribution and should be taken into account. The use of vibrational averaging and vibrational corrections is not limited to OR and has been used to produce more accurate values for one-electron properties such as polarizabilities, spin−spin coupling constants, nuclear magnetic shielding constants as well as thermochemistry calculations.[36−47] Pertaining to OR, past studies have shown that the zero-point vibrational correction can be as large as 20−30% compared to the electronic contribution to the OR.[48] It has also been shown that as the electronic contribution to the OR increases, the vibrational correction increases.[49] Within this work, the vibrational correction is used as a tool to evaluate the effect of isotopic substitution on the optical rotation.[48,49] Specifically, we examine how changing the location of H → D substitution affects the vibrational correction and which vibrations are large contributors. We rationalize these effects using a decomposition analysis of the OR in terms of occupied-virtual molecular orbital transitions[50−54] and we investigate how they change along vibrational coordinates before and after isotopic substitutions.

The paper is organized as follows. Section 2 reviews the most important theoretical concepts utilized in the simulations, while section 3 provides technical details of the simulations. The results are presented in section 4, and an analysis of these results is discussed in section 5. A summary of the main outcomes of this study and concluding remarks are reported in section 6.

2. THEORY

In this section, we briefly review the main theoretical concepts utilized in the simulations discussed in the following sections. The optical rotation of plane-polarized light as it passes through an isotropically dispersed chiral sample can be expressed as the specific rotation $[\alpha]_\omega$ (deg [dm (g/mL)]$^{-1}$), i.e., the OR normalized for path length and concentration of the sample:[55,56]

$$[\alpha]_\omega = \frac{(72 \times 10^6)\hbar^2 N_A \omega^2}{c^2 m_e^2 M} \frac{\mathrm{Tr}(\boldsymbol{\beta})}{3} \tag{1}$$

where the laser frequency ω is in atomic units, N_A is Avogadro's number, M is the molar mass in amu, m_e is the electron rest mass in kg, c is the speed of light (m/s), and $\hbar$ is the reduced Planck's constant (J s). The electric dipole-magnetic dipole polarizability tensor $\boldsymbol{\beta}$ can be evaluated using the linear-response formalism (LR).[2,12,18]

The measured OR is a combination of electronic and nuclear effects. Since the former are usually dominant, the total OR can be written as the sum of two separate terms:

$$[\alpha]_{tot} = [\alpha]_{eq} + [\alpha]_V \tag{2}$$

where $[\alpha]_{eq}$ from eq 1 is evaluated with LR theory at the equilibrium geometry and the nuclear contribution is introduced with perturbation theory as a zero-point vibrational correction over normal modes:[37,48,49]

$$\begin{aligned}[\alpha]_V &= \sum_{i=1}^{N_m} \frac{-1}{4\omega_i^2\sqrt{\bar{m}_i}}\left(\frac{\partial[\alpha]}{\partial Q_i}\right) \sum_{j=1}^{N_m} \frac{k_{ijj}}{\omega_j \bar{m}_j \sqrt{\bar{m}_i}} \\ &\quad + \sum_{i=1}^{N_m} \frac{1}{4\omega_i \bar{m}_i}\left(\frac{\partial^2[\alpha]}{\partial Q_i^2}\right) \\ &= \sum_{i=1}^{N_m} [\alpha]_{V1,i} + \sum_{i=1}^{N_m} [\alpha]_{V2,i} = [\alpha]_{V1} + [\alpha]_{V2}\end{aligned} \tag{3}$$

where Q_i represents the (nonmass weighted) normal coordinate for normal mode i, m_i represents the reduced mass, ω_i represents the frequency, N_m is the number of normal modes, and k_{ijj} is the anharmonic cubic force constant. Q_i, m_i, ω_i, and k_{ijj} are all expressed in atomic units and eq 3 is multiplied by an implicit factor of $\hbar$ = 1 au, which ensures the resulting units for $[\alpha]_{V1}$ and $[\alpha]_{V2}$ are the same as those for $[\alpha]_{eq}$. The second line in eq 3 emphasizes the contribution of individual vibrational normal modes to two main terms: $[\alpha]_{V1}$, which is the anharmonic contribution that arises from the difference between the equilibrium and effective geometries, and $[\alpha]_{V2}$, which depends on the curvature of the property surface. We will quantify the effect of isotopic substitution in terms of $[\alpha]_V$ in eq 3. However, in the normal mode representation, the motion of a particular atom can contribute to a large number of different modes. This spreads the effect of isotopic substitution over multiple modes. In addition, each of these modes potentially involves all other atoms in the molecule, making it challenging to determine what atomic motion is driving the change in vibrational contribution. Both of these issues can be alleviated by employing localized vibrational modes. A localized mode will only involve the motion of a small number of nearby atoms, making it easier to isolate what atomic motion is causing a change in vibrational contribution. A particular atom in turn only contributes to a small number of local modes in its vicinity. We use the Pipek-Mezey scheme, which is typically used to localize molecular orbitals (it maximizes the sum of squares of atomic contributions to orbitals). The method can also be applied to maximize the sum of squares of atomic contributions to vibrational modes.[57,58] The Pipek-Mezey transformation from normal to local modes is defined in terms of a unitary matrix, $\mathbf{U}$, and we can use this matrix to express the components of $[\alpha]_V$ in terms of local mode contributions. First, we introduce two auxiliary matrices, whose diagonal elements correspond to $[\alpha]_{V1,i}$ and $[\alpha]_{V2,i}$ from eq 3:

$$M_{ij}^{V1} = \frac{-1}{4\omega_i^2\sqrt{\bar{m}_i}}\left(\frac{\partial[\alpha]}{\partial Q_i}\right) \sum_{l=1}^{N_m} \frac{k_{jll}}{\omega_l \bar{m}_l \sqrt{\bar{m}_j}} \rightarrow M_{ii}^{V1} \equiv [\alpha]_{V1,i} \tag{4}$$

$$M_{ij}^{V2} = \frac{1}{4\sqrt{\omega_i \bar{m}_i \omega_j \bar{m}_j}}\left(\frac{\partial^2[\alpha]}{\partial Q_i \partial Q_j}\right) \rightarrow M_{ii}^{V2} \equiv [\alpha]_{V2,i} \tag{5}$$

such that $\mathrm{Tr}(\mathbf{M}^{Vk}) = [\alpha]_{Vk}$, with k = 1, 2. By unitarily transforming the matrices in eqs 4 and 5 with $\mathbf{U}$, we convert the normal mode to local mode contributions. The unitary transformation preserves the trace of these matrices and thus the values of $[\alpha]_{V1}$ and $[\alpha]_{V2}$. Furthermore, the diagonal elements of the transformed matrices can be taken as the individual local mode contributions to $[\alpha]_{V1}$ and $[\alpha]_{V2}$, equivalent to the sums over vibrational modes in the second line of eq 3.

https://doi.org/10.1021/acs.jpca.4c03728
J. Phys. Chem. A 2024, 128, 8045−8059

In order to evaluate the electronic effect of the isotope substitution on the OR, we use an analysis tool developed in our group. The OR can be decomposed into transitions within the molecular orbital space by introducing a rotatory strength in configuration space, $\tilde{S}_{ia}$:[50−54]

$$\tilde{S}_{ia} = \mathrm{Im}[\langle i|\boldsymbol{\mu}|a\rangle \cdot \langle a|\mathbf{X}_{\mathbf{m}}^{+}|i\rangle] \tag{6}$$

where i/a indicate occupied/virtual molecular orbitals (MOs), respectively, $\langle i|\boldsymbol{\mu}|a\rangle$ are the electric dipole integrals in MO basis and $\langle a|\mathbf{X}_{\mathbf{m}}^{+}|i\rangle$ are the magnetic perturbed density elements from the LR calculation. The $\tilde{S}_{ia}$ values in eq 6 are related to the OR as

$$\sum_{ia} \tilde{S}_{ia} = \omega \mathrm{Tr}(\boldsymbol{\beta}) \tag{7}$$

3. COMPUTATIONAL METHODS

The equilibrium geometry of the chosen molecules as well as the properties ($[\alpha]_{eq}$, $[\alpha]_V$, $\tilde{S}_{ia}$) were calculated at the B3LYP/aug-cc-pVDZ level of theory.[59,60] Calculations were performed off-resonance at a perturbation wavelength of 589.3 nm using a development version of the GAUSSIAN suite of programs.[61] Visualizations of the electric and magnetic dipole vectors of the one-electron transitions were generated using PyMOL.[62] The importance of the vibrational correction to the OR and the changes due to isotopic substitution are analyzed in terms of the relative quantities Δ^{Rel} and $\Delta\Delta^{Rel}$, defined as (see eqs 2 and 3):

$$\Delta^{Rel} = \frac{[\alpha]_{tot} - [\alpha]_{eq}}{[\alpha]_{eq}} = \frac{[\alpha]_V}{[\alpha]_{eq}}$$

$$\Delta\Delta^{Rel} = \frac{[\alpha]_{VS} - [\alpha]_{VU}}{[\alpha]_{eq}} \tag{8}$$

where VU and VS refer to the vibrational correction of the unsubstituted and isotopically substituted molecule, respectively.

The molecules used in the study are presented in a compact notation in Figure 1. The structure and nomenclature for each compound are reported in Figures S1−S7 in the Supporting Information (SI). All optimized geometries are also reported in the SI in xyz file format. The $[\alpha]_{eq}$, $[\alpha]_{V1}$, and $[\alpha]_{V2}$ values for all molecules and all isotopologues are reported in Tables S1−S7 of the SI. These molecules were chosen because they are similar in structure, small (to limit the number of vibrational degrees of freedom), and rigid (to avoid the need for conformational analysis). Additionally, only molecules that are optically active prior to isotopic substitution were chosen such that we can define the relative quantities in eq 8 (we chose the enantiomers with a positive value of $[\alpha]_{eq}$ for convenience, as this term appears at the denominator in the equation). The choice of X moieties and R groups provides a range of electron-donating or electron-withdrawing behavior and electron density polarization. The term diastereomer in Figure 1 refers to the change in the X-Y stereochemistry (see Figures S1−S7 in the SI). The majority of this study focuses on a single H → D substitution, although we will present some results for double substitutions. There are several diastereomers that have disproportionately high $\Delta\Delta^{Rel}$ values because they have a small equilibrium OR, $[\alpha]_{eq}$ < 28 deg [dm (g/mL)]$^{-1}$): PCl-2Me, PCl-F-Me-Diast.1, PH-1Me-Diast.1, PH-1F-Diast.1, O-1F, O-2F, O-1Me, NBr-2Me, and NCl-2Me, see Figures S1−S7 and the corresponding Tables S1−S7 in the SI for their structure and $[\alpha]_{eq}$ values. These molecules were not included in the data reported in Figures 2−4, based on relative values with $[\alpha]_{eq}$ at denominator, see eq 8, to avoid skewing the results for certain X groups.

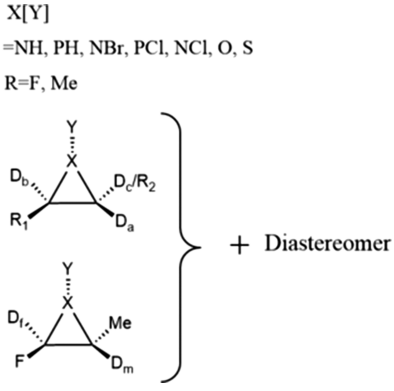

Figure 1. Diagram of test set molecules. D_a, D_b, D_c, D_l, and D_m represent prospective locations of single isotopic substitution.

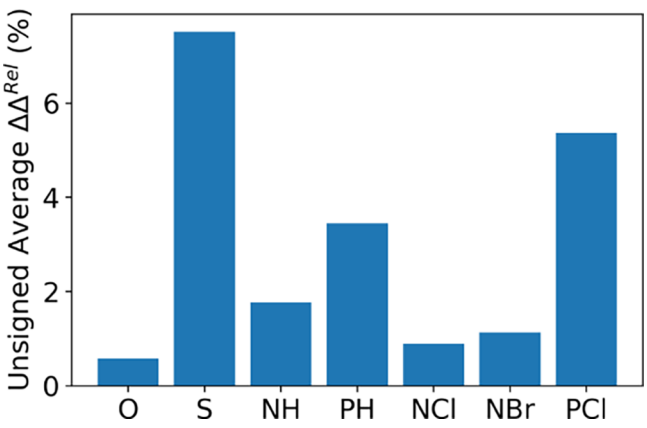

Figure 2. Unsigned average $\Delta\Delta^{Rel}$ for test set of molecules divided by X group. Each average includes molecules with separate D_a, D_b, D_c, D_m, and D_f with all permutations of R identity and orientation of Y.

The localization procedure of vibrational modes discussed in section 2 works better when normal modes of similar nature are grouped together. Specifically, we separate hydrogen stretching from the rest (coupled heteroatom/carbon/hydrogen vibrations). Hydrogen stretching modes were localized by selecting the normal modes of the parent molecule at frequencies larger than 3000 cm^{-1}. The same modes were also selected after isotopic substitution, irrespective of the change in frequency. The remaining modes were considered together in the localization procedure and this produced carbon stretching, hydrogen wagging, and stretching and wagging of the functional groups.

As discussed in section 2, we utilize the OR $\tilde{S}_{ia}$ decomposition, see eqs 6 and 7, to examine which occupied-virtual MOs transition pairs are significant during vibrations (with normal and localized modes).[50,51,53,54] Specifically, we use a numerical differentiation of the $\tilde{S}_{ia}$ values to examine which orbital pairs are affected the most by changes in the equilibrium geometry along normal and local coordinates. This

https://doi.org/10.1021/acs.jpca.4c03728
J. Phys. Chem. A 2024, 128, 8045−8059

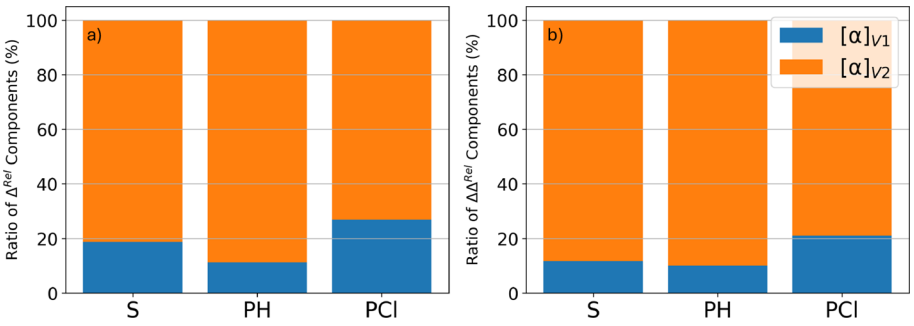

Figure 3. Ratio of average $[\alpha]_{V1}$ and $[\alpha]_{V2}$ contributions to overall Δ^{Rel} (percent) in (a). Ratio of average $[\alpha]_{V1}$ and $[\alpha]_{V2}$ contributions to overall $\Delta\Delta^{Rel}$ (percent) in (b).

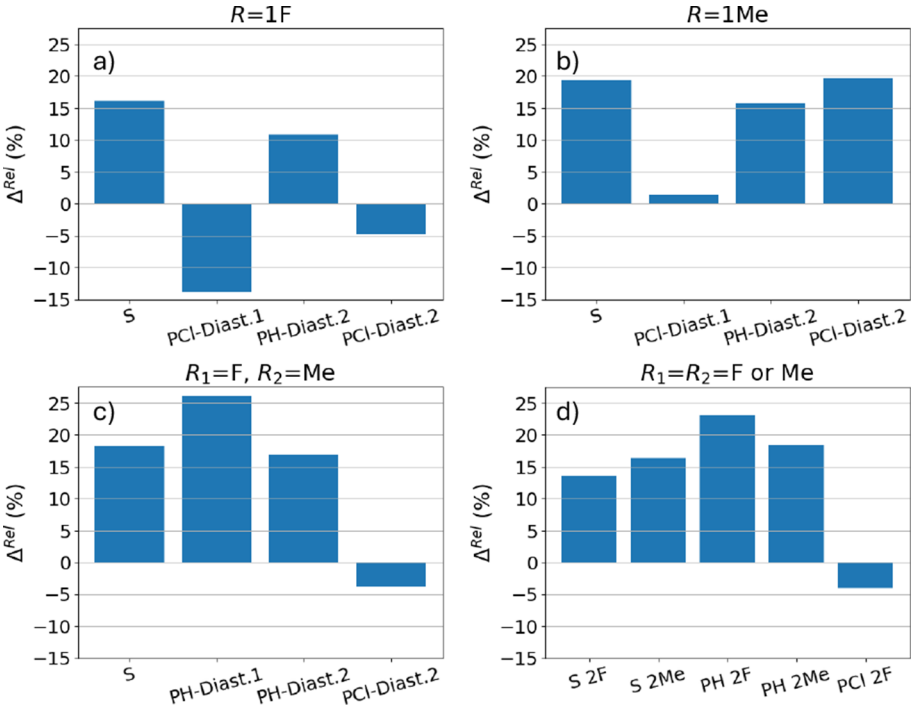

Figure 4. Δ^{Rel} (percent) values for unsubstituted molecules with different substituent groups: (a) R = F, (b) R = Me, (c) R_1 = F, R_2 = Me, and (d) R_1 = R_2 = F or Me.

effect can be quantified with expressions similar to Δ^{Rel} and $\Delta\Delta^{Rel}$ in eq 8:

$$\Delta\tilde{S}_{ia} = \frac{\tilde{S}_{+} - \tilde{S}_{-}}{\sum \tilde{S}_{eq}}$$

$$\Delta\Delta\tilde{S}_{ia} = \frac{(\tilde{S}_{+} - \tilde{S}_{-})_S - (\tilde{S}_{+} - \tilde{S}_{-})_U}{\sum \tilde{S}_{eq}} \quad (9)$$

Here, the plus and minus signs denote the $\tilde{S}_{ia}$ values for the forward and backward displacements, respectively. As the vibrational corrections are evaluated with respect to the first and second property derivatives, we verified that the finite difference approach gives the same sign as the analytically derived derivatives for $[\alpha]_V$ along each mode. An important aspect of finite difference methods is the choice of step size.[10,48,63] Given that the $\tilde{S}_{ia}$ analysis is qualitative in nature, we found that a single step size of 0.00521 (this is the fraction of the normalized displacement vectors used to displace the molecule) was sufficiently accurate for each normal mode across multiple molecules. For localized modes it was difficult to find a displacement that worked well for all molecules, and the best step size was 0.008 for the *PCl − 1F − Diast.*2 molecule and 0.004 for the *PCl − 1Me − Diast.*2 molecule (although it is worth noting that for a relatively wide range of step sizes the qualitative behavior of the MO transitions for each mode was the same). A subset of vibrational modes was chosen that has a large change in $[\alpha]_V$.

4. RESULTS

In this section, we analyze the vibrational corrections of the test set of molecules, shown in Figure 1. First, we determine which X functional groups provide the largest $\Delta\Delta^{Rel}$ values, see eq 8. The unsigned average $\Delta\Delta^{Rel}$ value across all molecules and isotopologues with the same X group is presented in Figure 2. Molecules with larger and more polarizable X groups have the largest unsigned $\Delta\Delta^{Rel}$ average. The effect is due to the heteroatom in the ring, not the Y atom, as seen with the relatively small values of NCl and NBr. Therefore, in the following we limit the discussion to the three groups with the largest isotope effect: S, PH, and PCl. In order to understand whether $[\alpha]_{V1}$ or $[\alpha]_{V2}$ contribute the most to both the

https://doi.org/10.1021/acs.jpca.4c03728
J. Phys. Chem. A 2024, 128, 8045−8059

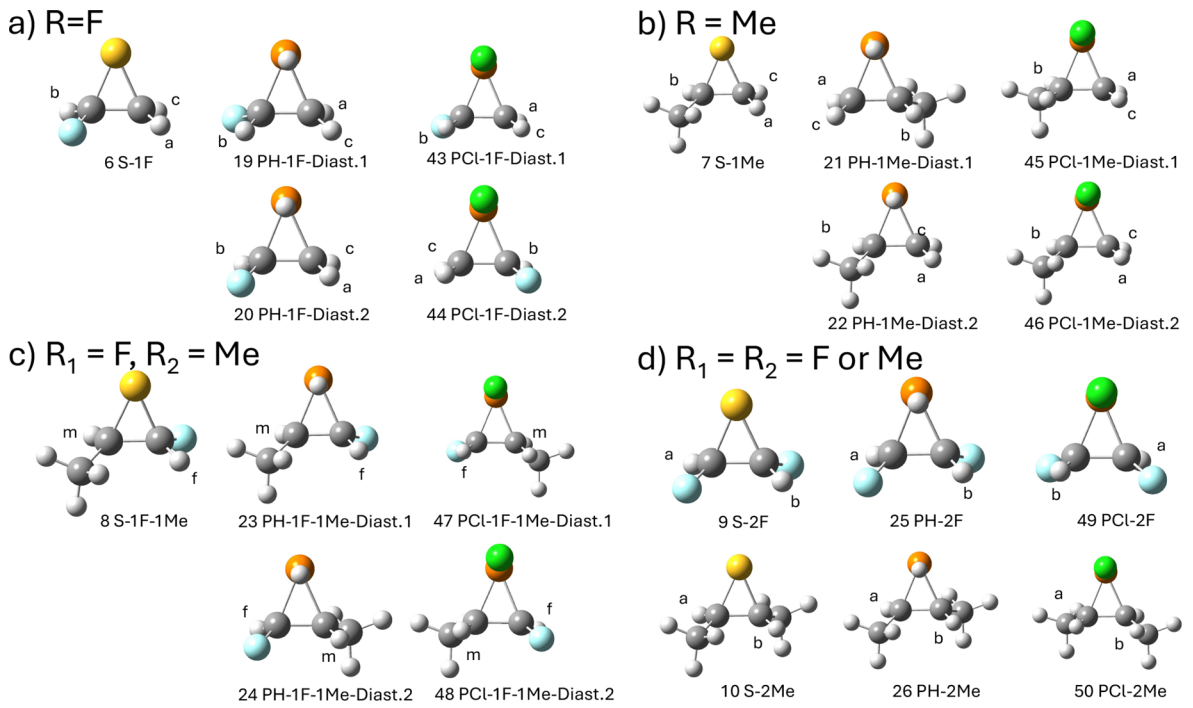

Figure 5. Structures of the compounds discussed in Figure 4. The compounds are divided into four categories based on their R group: (a) R = F, (b) R = Me, (c) R_1 = F, R_2 = Me, and (d) R_1 = R_2 = F or Me. Name and numbering follow the nomenclature outline in Figures S1−S7 of the SI.

vibrational correction of the unsubstituted molecule (Δ^{Rel}) as well as the change of $[\alpha]_V$ between substituted and unsubstituted molecules ($\Delta\Delta^{Rel}$), we plot their relative contributions in Figure 3. Even though there is some variation across X groups, it is evident that $[\alpha]_{V2}$ is the major contributor to the vibrational correction and its change due to isotopic substitution.

Although the main interest is in the effect of the isotopic substitution, it is instructive to examine the Δ^{Rel} values for each individual R group and diastereomer of the unsubstituted molecules, reported in Figure 4. The structures of the corresponding parent compounds are reproduced in Figure 5. These plots indicate that the effect of X and R groups as well as their stereochemistry is significant. For example, the difference between *PCl − Diast.*1 and *PCl − Diast.*2 is around 15% for R = Me. One pattern that emerges from Figure 4 is that whenever a fluorine atom and the PCl moiety are on the same side with respect to the plane of the ring, $[\alpha]_V$ and Δ^{Rel} are negative. This is seen for *PCl − Diast.*2 in Figure 4a, for *PCl − Diast.*2 in (c), and for *PCl − 2F* in (d). For R = F or Me, the vibrational correction is negative for diastereomer 2, although this corresponds to the fluorine atom on the same side as the PCl moiety and the methyl group on the opposite side of the plane of the ring. This is the same for R_1 = R_2 = F or Me. Even in the case of *PCl − 1F − Diast.*1, where the fluorine is on the opposite side of the plane of the ring as the chlorine, there is a negative vibrational correction.

Figure 6 reports the $\Delta\Delta^{Rel}$ percent values based on location of isotopic substitution for individual X and R groups. The molecules with a single R group tend to have larger $\Delta\Delta^{Rel}$ values compared to those with two R groups, for instance for X = S, compare the results for R = F or Me versus those for R_1 = F, R_2 = Me. Isotopic substitutions made to hydrogens bonded to the same carbon (see D_a and D_c in Figure 5) always result in $\Delta\Delta^{Rel}$ values with different signs. This can be understood considering a hypothetical axis of rotation that passes through

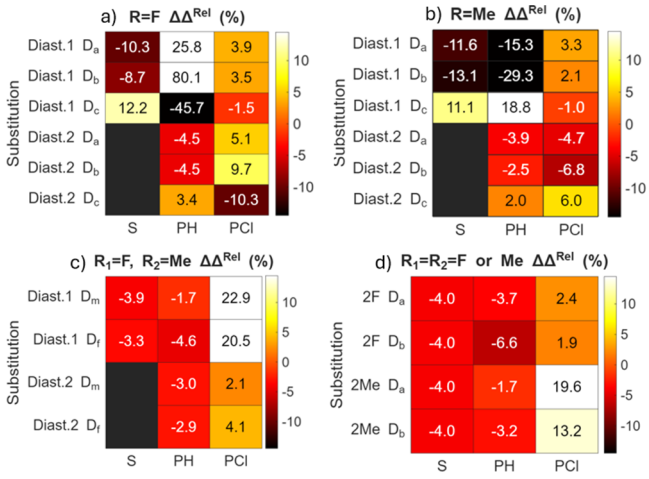

Figure 6. $\Delta\Delta^{Rel}$ (percent) heatmaps for different isotopic substitution locations. These plots are divided into four categories based on their R group: (a) R = F, (b) R = Me, (c) R_1 = F, R_2 = Me, and (d) R_1 = R_2 = F or Me, see Figure 5 for the structure.

the heteroatom and the middle of the CC bond in the ring. Isotopic substitutions on the same C would correspond to opposite handedness with respect to this axis. Using the same argument, it is clear why isotopic substitutions made to hydrogens bonded to different carbons and on the opposite side of the ring plane (D_a and D_b) result in $\Delta\Delta^{Rel}$ values with the same sign. When the R and Y groups are on the same side with respect to the plane of the ring, the molecules exhibit different $\Delta\Delta^{Rel}$ behavior with respect to a change in R group. For the PH group, $\Delta\Delta^{Rel}$ has the same sign for R = F and Me, while its sign changes for the PCl group. Molecules with the sulfur heteroatom have the same signs for each deuterium location for both R groups. When there are R groups on both sides of the molecule, the $\Delta\Delta^{Rel}$ values are all negative for both

https://doi.org/10.1021/acs.jpca.4c03728
J. Phys. Chem. A 2024, 128, 8045−8059

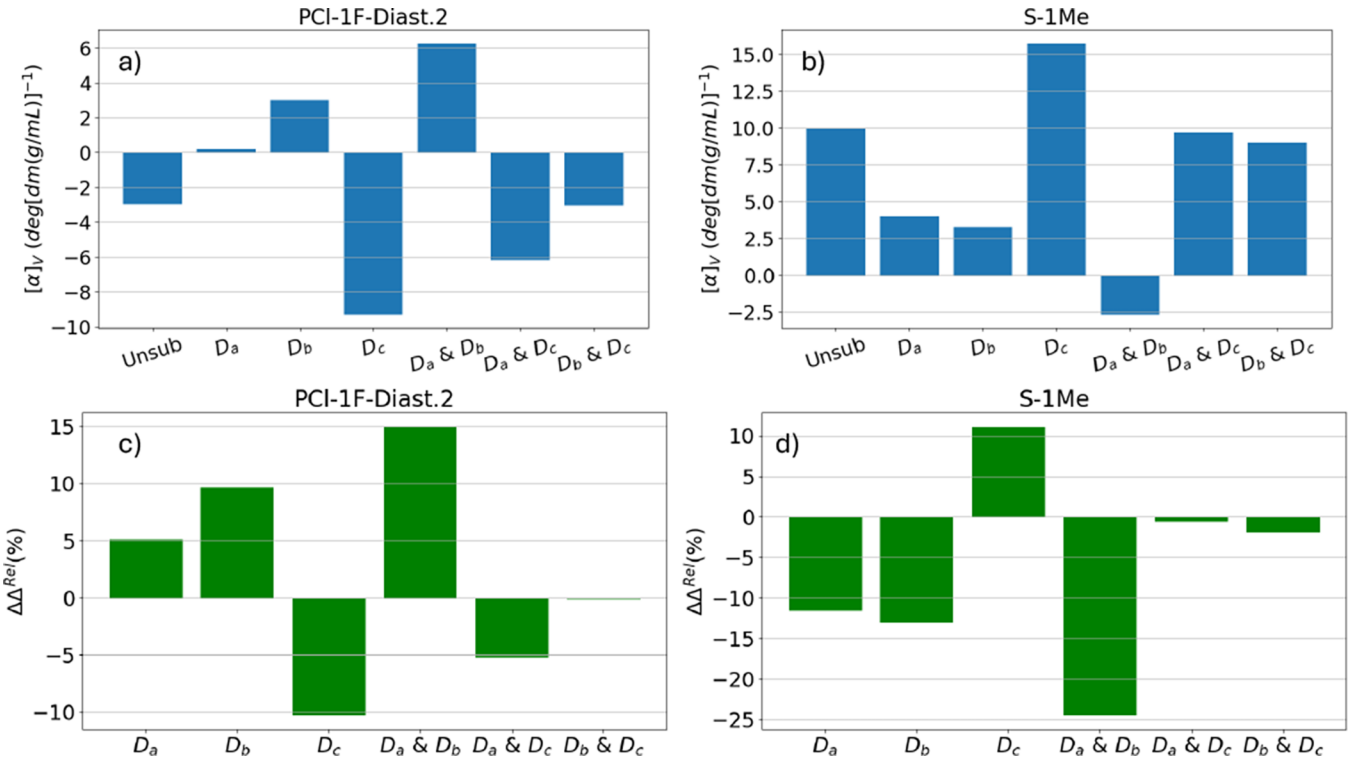

Figure 7. $[\alpha]_V$ deg [dm (g/mL)]$^{-1}$ for single and double isotopic substitution presented in (a) and (b) for $PCl-1F-Diast.2$ and $S-1Me$. $\Delta\Delta^{Rel}$ values presented in (c) and (d).

the S and PH moieties (irrespective of which side of the ring the PH is directed). On the other hand, all of the values are positive for the PCl group, irrespective of which side of the ring the chlorine atom is. These values also tend to be lower in magnitude compared to when there is a single R group.

While the previous figures consider only one deuterium atom at a time, Figure 7 presents $[\alpha]_V$ and $\Delta\Delta^{Rel}$ values for two molecules with isotopic substitution at two locations simultaneously. The bars labeled D_i & D_j represents the vibrational correction for the doubly substituted molecules at positions i and j. The $[\alpha]_V$ plots indicate that the effect of isotopic substitution is not directly additive. For instance, the plot in Figure 7a shows positive vibrational corrections for the molecules with isotopic substitutions D_a and D_b, but when both are substituted, the resulting correction is greater than the sum of the individual values. Conversely, Figure 7b shows that having two deuterium atoms results in a negative vibrational correction even if the individual deuterium substitutions have positive vibrational corrections, albeit smaller than the unsubstituted molecule. This pattern can be explained by examining the $\Delta\Delta^{Rel}$ values in Figure 7c,d. These plots show that it is the $\Delta\Delta^{Rel}$ value, i.e., the change in vibrational correction with isotopic substitution, that is approximately additive rather than the $[\alpha]_V$ itself.

4.1. Vibrational Analysis. We can now analyze the contribution of individual vibrational modes to $[\alpha]_{V1}$ and $[\alpha]_{V2}$ according to eq 3. We limit this discussion to the $S-1F$, $S-1Me$, $PCl-1F-Diast.2$, and $PCl-1Me-Diast.2$ molecules because they have the largest $\Delta\Delta^{Rel}$ values (and an equilibrium OR greater than 28 deg [dm (g/mL)]$^{-1}$), see Figures 5 and 6. Since the nature of the normal modes can change with isotopic substitution, it is not possible to make a one-to-one comparison across individual modes in this basis. Therefore, the vibrational contributions of individual normal modes in terms of $[\alpha]_{V1}$ and $[\alpha]_{V2}$ is shown in Figures S8 and S9 of the SI, respectively, with a brief discussion of the data.

A more effective way to examine vibrational contributions as a result of isotopic substitution is to focus on localized modes, as they are more easily comparable across isotopologues. It is convenient to introduce the labeling that will be used as well as visualizations of many of the localized modes, presented in Figure 8. This labeling allows for the grouping and comparison of localized modes across different R and X[Y] groups. After the localization procedure, there are two wagging modes for each hydrogen atom and one stretching mode for each hydrogen atom. The number of carbon stretching modes depends on whether the X group is PCl or S. For PCl, there are

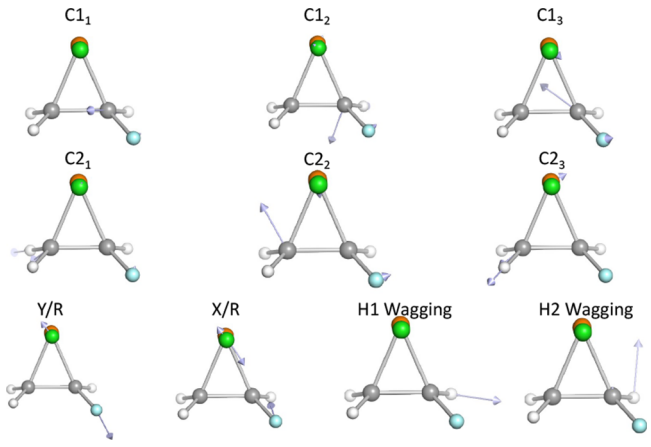

Figure 8. Labeling and displacement vectors for localized modes. The plots were produced with the PyVibMS[64] plugin for the PyMOL software.[62]

https://doi.org/10.1021/acs.jpca.4c03728
J. Phys. Chem. A 2024, 128, 8045−8059

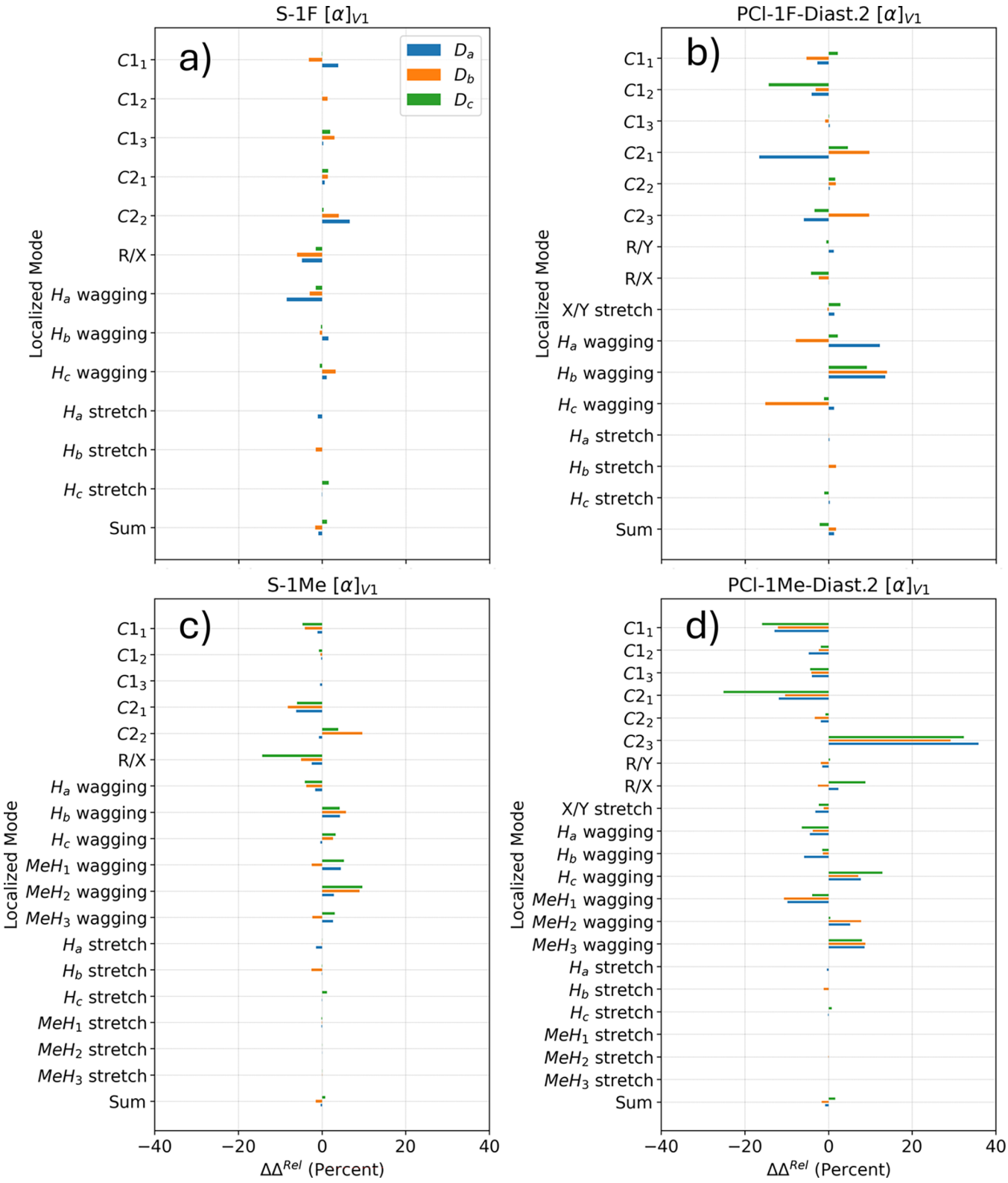

Figure 9. $\Delta\Delta^{Rel}$ (percent) values for $[\alpha]_{V1}$ of localized modes for four molecules: (a) $S-1F$, (b) $PCl-1F-Diast.2$, (c) $S-1Me$, and (d) $PCl-1Me-Diast.2$.

three $C2$ localized vibrations, and in terms of S-containing molecules, there are two $C2$ localized vibrations (see Figure 8).

Contrary to normal modes, the behavior of the localized modes is qualitatively the same for all isotopologues. The vibrational correction of the localized vibrational modes is presented in Figures S10 and S11 in the SI, with some discussion of the data. Here, we report the corresponding $\Delta\Delta^{Rel}$ values, presented in Figures 9 and 10 for $[\alpha]_{V1}$ and $[\alpha]_{V2}$, respectively, because they facilitate the analysis. One interesting category of localized modes are the hydrogen

https://doi.org/10.1021/acs.jpca.4c03728
J. Phys. Chem. A 2024, 128, 8045−8059

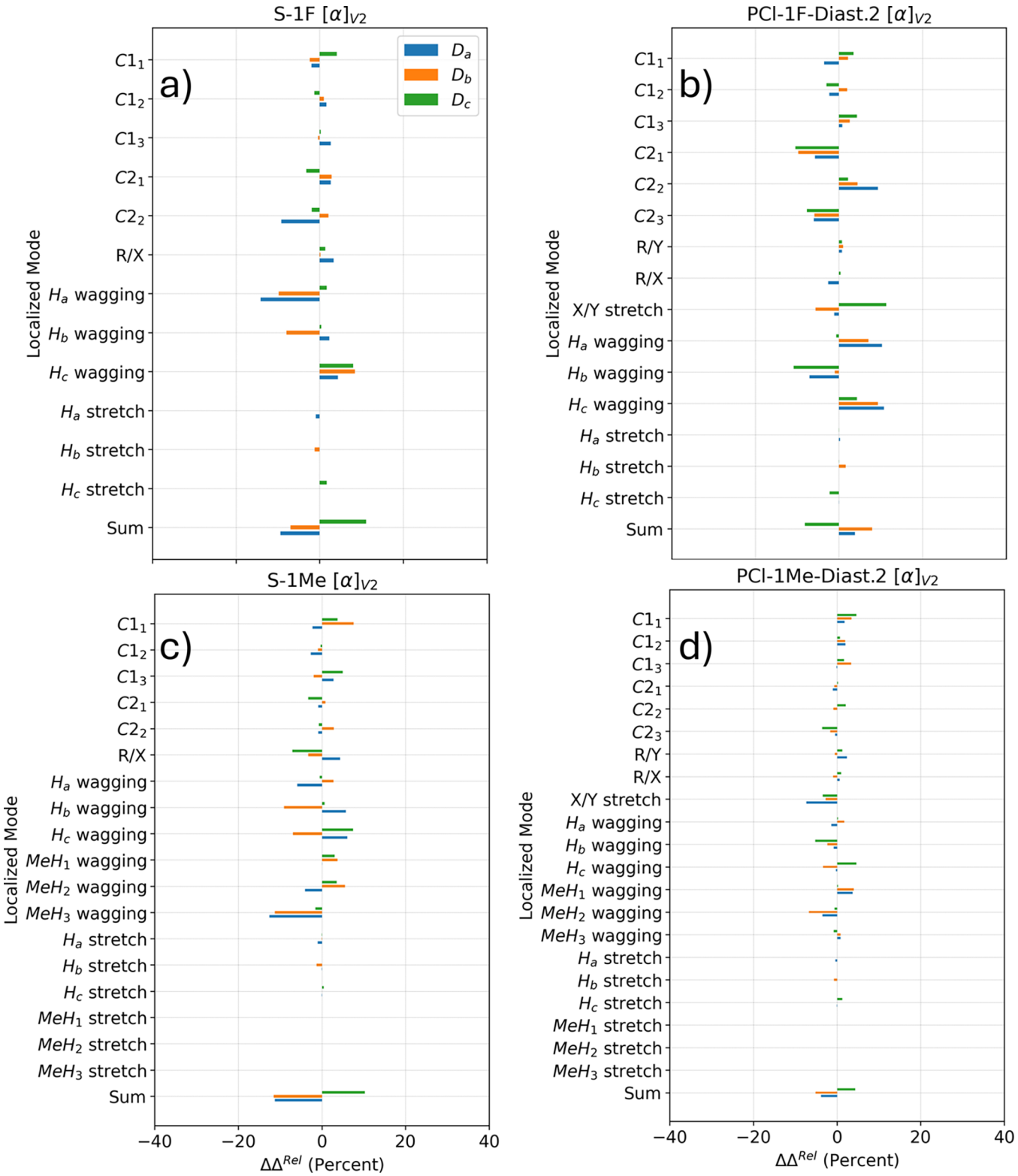

Figure 10. $\Delta\Delta^{Rel}$ (percent) values for $[\alpha]_{V2}$ of localized modes for four molecules: (a) $S-1F$, (b) $PCl-1F-Diast.2$, (c) $S-1Me$, and (d) $PCl-1Me-Diast.2$.

stretching modes. These modes have small $\Delta\Delta^{Rel}$ values, which is somewhat unexpected given that the different mass of the deuterium atom affects the frequency of the stretching. At most, the $\Delta\Delta^{Rel}$ value for the stretching of D_c for $PCl-1F-Diast.2$ is −2%. On the other hand, hydrogen wagging modes appear to be significant contributors to the change in $[\alpha]_V$ as a result of isotopic substitution. In Figures 9 and 10a, c, and d, the isotopic substitution of the atom wagging results in a vibration with $[\alpha]_V$ smaller in magnitude, which corresponds to a negative $\Delta\Delta^{Rel}$ for D_a and D_b and a positive $\Delta\Delta^{Rel}$ for D_c. Also in Figures 9 and 10, the molecule in (b) ($PCl-1F-Diast.2$) is unique because D_a, D_b, and D_c wagging modes all

https://doi.org/10.1021/acs.jpca.4c03728
J. Phys. Chem. A 2024, 128, 8045−8059

have positive $\Delta\Delta^{Rel}$ values. In Figure 9d, the carbon stretching modes also appear to be significant contributors to $\Delta\Delta^{Rel}$. For the three isotopologues of *PCl* − 1*Me* − *Diast*.2, the qualitative behavior is the same for these six modes: they all have negative $\Delta\Delta^{Rel}$ values except for $C2_3$.

4.2. Occupied-Virtual MO Transitions. The $\tilde{S}_{ia}$ analysis was performed in order to determine the contributing one-electron MO transitions that are most influenced by isotopic substitution along the normal and localized coordinates for two representative molecules: *PCl* − 1*F* − *Diast*.2 and *PCl* − 1*Me* − *Diast*.2, see Figure 5. Figure 11 presents the $\tilde{S}_{ia}$ heatmap for

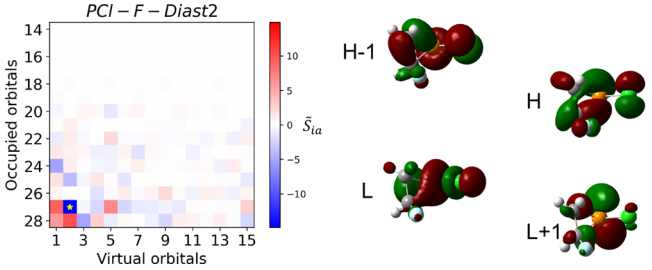

Figure 11. $\tilde{S}_{ia}$ of *PCl* − 1*F* − *Diast*.2 at equilibrium geometry and visualizations of HOMO−1, HOMO, LUMO, LUMO+1 molecular orbitals. The ∗ denotes the largest transition.

the parent molecule at equilibrium geometry as well as visualizations for four of the frontier molecular orbitals. The OR can be mainly characterized by relatively few transitions, thus only the highest 15 occupied orbitals and lowest 15 virtual orbitals are presented in each figure.[53] In order to provide a physical interpretation of these one-electron transitions, PyMOL software was used for the visualization of the transitions in terms of electric and magnetic dipole density vectors, shown in Figure 12. The transitions to the LUMO+1

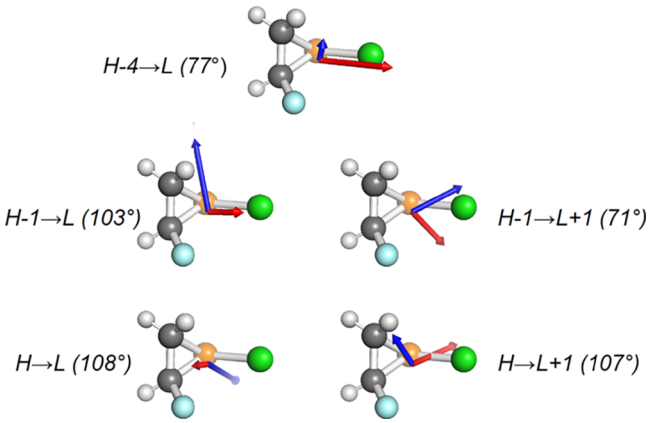

Figure 12. Visualization of electric dipole (red) and magnetic dipole (blue) density vectors at equilibrium geometry for prominent *PCl* − 1*F* − *Diast*.2 $\tilde{S}_{ia}$ transitions. The numbers in parentheses are the angles between the vectors.

virtual orbital involve prominent charge transfer from the chlorine atom to the phosphorus. The HOMO−1 and HOMO → LUMO transitions involve significant rotation of charge, as displayed by the magnetic dipole density vectors. The HOMO−1 → LUMO+1 transition features significant orbital rotation as well as electron density transferring from the chlorine atom to the phosphorus atom.

As discussed in section 4.1, normal modes are difficult to compare between isotopologues. Nonetheless, the analysis of $\Delta\tilde{S}_{ia}$ values (as defined in eq 9) for a few significant vibrations of the unsubstituted molecule is reported in the SI (Figure S12). For localized modes, we focus on two H_a and two H_b wagging modes and a *C*1 vertical carbon stretching mode as representative modes of D_a and D_b's positive $\Delta\Delta^{Rel}$ and D_c's negative $\Delta\Delta^{Rel}$, as shown in Figures 9 and 10. The $\Delta\tilde{S}_{ia}$ analysis for these modes is reported in the SI (Figure S13). The main result of these analyses is that the largest contributors to $\Delta\tilde{S}_{ia}$ are the same main transitions that define the $\tilde{S}_{ia}$ heatmap in Figure 11.

More interestingly for this discussion, Figure 13 reports how $\Delta\tilde{S}_{ia}$ values change with isotopic substitutions, which we called $\Delta\Delta\tilde{S}_{ia}$ in eq 9 in analogy to the notion of $\Delta\Delta^{Rel}$. In Figure 13, the largest values are mostly found among the four frontier orbitals. Thus, the same orbital transitions that are relevant at equilibrium (Figure 11), and $\Delta\tilde{S}_{ia}$ for normal and localized modes (Figures S12 and S13 in the SI) are also the most important for $\Delta\Delta\tilde{S}_{ia}$. In Figure 13a, b, and d, three of the four hydrogen wagging localized modes possess the greatest $\Delta\Delta\tilde{S}_{ia}$ value for the HOMO → LUMO transition, which involves rotation of charge around the PCl group. These modes can be contrasted with Figure 13c, where the H_b1 wagging localized mode possesses the greatest $\Delta\Delta\tilde{S}_{ia}$ value for the HOMO−1 → LUMO+1 transition. The only carbon vibration chosen for this molecule, presented in Figure 13 e), possesses the greatest $\Delta\Delta\tilde{S}_{ia}$ value for the HOMO → LUMO+1 transition. The isotopic substitution of D_c can slightly change the displacement vector of the carbon bonded to the fluorine, thus, mostly affecting the linear flow of charge to the PCl group.

Although the most important transitions are the same, from $\tilde{S}_{ia}$ at equilibrium to $\Delta\Delta\tilde{S}_{ia}$, visualizing the changes in the orientation and magnitude of the transition dipoles in Figure 12 is difficult. Instead, we report relative changes in the magnitude of the transition dipoles and in the angle between them (with respect to the values at equilibrium) in Table 1, for the transitions of HOMO−1 → LUMO+1, HOMO → LUMO and LUMO+1. Since these values are unitless, they can be compared to each other and provide information on what quantity changes the most due to isotopic substitution (note that the values are relatively small due to the necessarily small step size in the numerical derivative). The change in the electric dipole magnitude is greater than for the magnetic dipole for two of the five transitions. These correspond to the same type of vibration between the two isotopologues, D_a1 and D_b1. The other three modes, D_a2, D_b2, and $C1_2$ experience the largest change in the cosine of the angle between the dipoles (i.e., in their relative orientation).

Figure 14 presents the $\tilde{S}_{ia}$ analysis for the *PCl* − 1*Me* − *Diast*.2 molecule at its equilibrium geometry. We can see that the OR can be characterized again by just a few transitions, mainly HOMO−1 and HOMO → LUMO+1. Figure 15 visualizes the transitions in terms of the electric dipole and magnetic dipole density vectors. This figure shows that transitions to the LUMO+1 virtual orbital exhibit significant electric dipole vectors, whereas transitions to the virtual LUMO exhibit significant magnetic dipole density vectors. The largest $\tilde{S}_{ia}$ value in Figure 14 is the HOMO → LUMO+1 transition that is characterized by charge flow along the ring to the phosphorus atom. More molecular orbitals and transitions are presented that are needed based off of the equilibrium heatmap in Figures 14 and 15 because they are relevant in the

https://doi.org/10.1021/acs.jpca.4c03728
J. Phys. Chem. A 2024, 128, 8045−8059

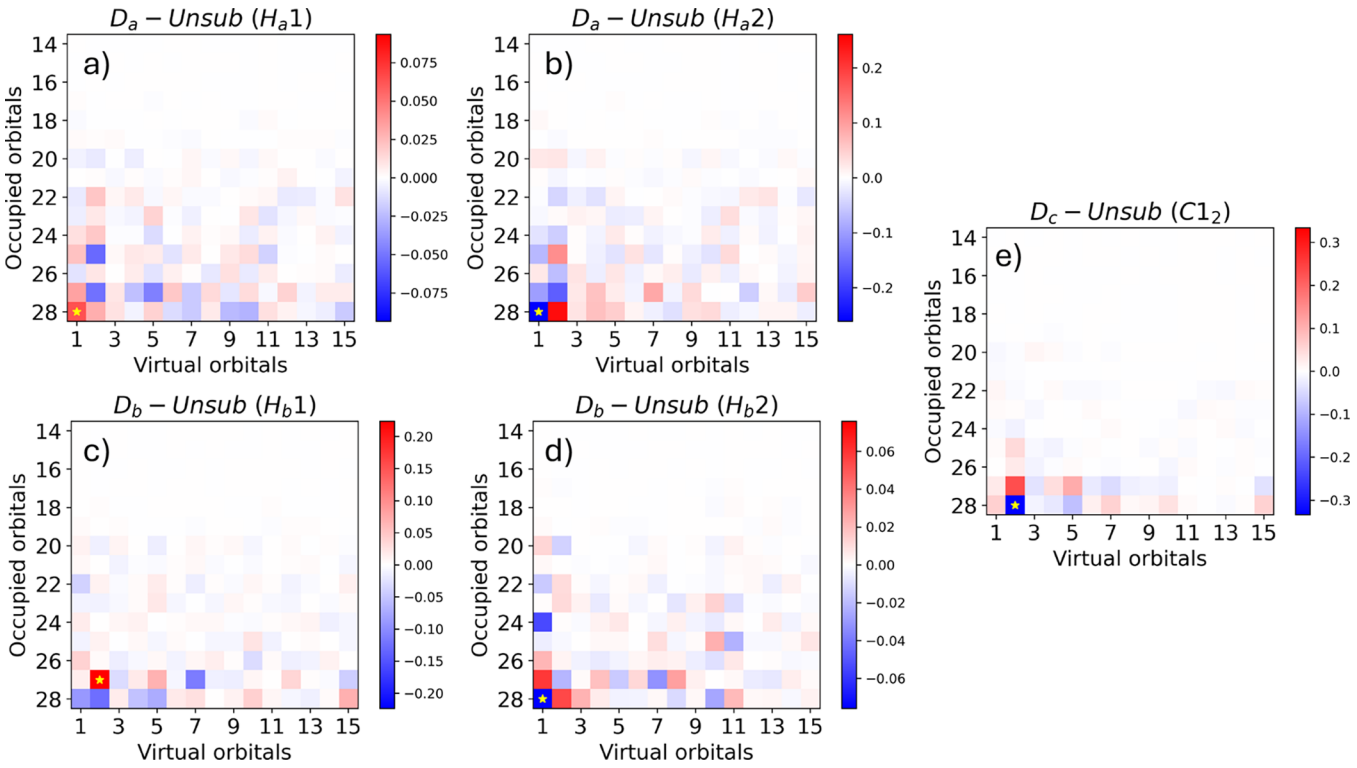

Figure 13. (a−e) $\Delta\Delta\tilde{S}_{ia}$ values normalized with respect to Tr($\boldsymbol{\beta}$) for *PCl* − 1*F* − *Diast*.2 localized modes. The ∗ denotes the largest transition.

Table 1. Decomposition of $\Delta\Delta\tilde{S}_{ia}$ Values into % Change of Electric Dipole Vector Magnitude ($|\boldsymbol{\mu}|$), Magnetic Dipole Density Vector Magnitude ($|\boldsymbol{m}|$) and the cos($\boldsymbol{\theta}$) of the Vectors for Selected *PCl* − 1*F* − *Diast*.2 Transitions[a]

localized mode	transition	$\Delta\Delta\lvert\mu\rvert$	$\Delta\Delta\lvert m\rvert$	$\Delta\Delta\cos(\theta)$
D_a1	HOMO → LUMO	0.66	0.21	0.22
D_a2	HOMO → LUMO	0.06	−0.21	−1.09
D_b1	HOMO−1 → LUMO+1	−0.68	−0.20	−0.63
D_b2	HOMO → LUMO	−0.05	0.07	−1.31
$C1_2$ (D_c)	HOMO → LUMO+1	0.14	−0.94	−2.46

[a]All values are normalized with respect to the corresponding quantity at the equilibrium geometry and valid for a step size of 0.008. The $C1_2$ values refer to the isotopic substitution of H_c.

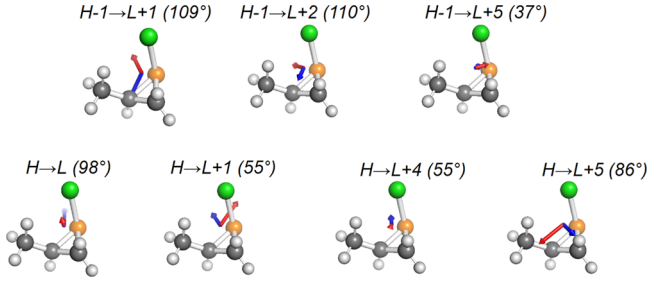

Figure 15. Visualization of electric dipole (red) and magnetic dipole (blue) density vectors at equilibrium geometry for prominent *PCl* − 1*Me* − *Diast*.2 $\tilde{S}_{ia}$ transitions. The numbers in parentheses are the angles between the vectors.

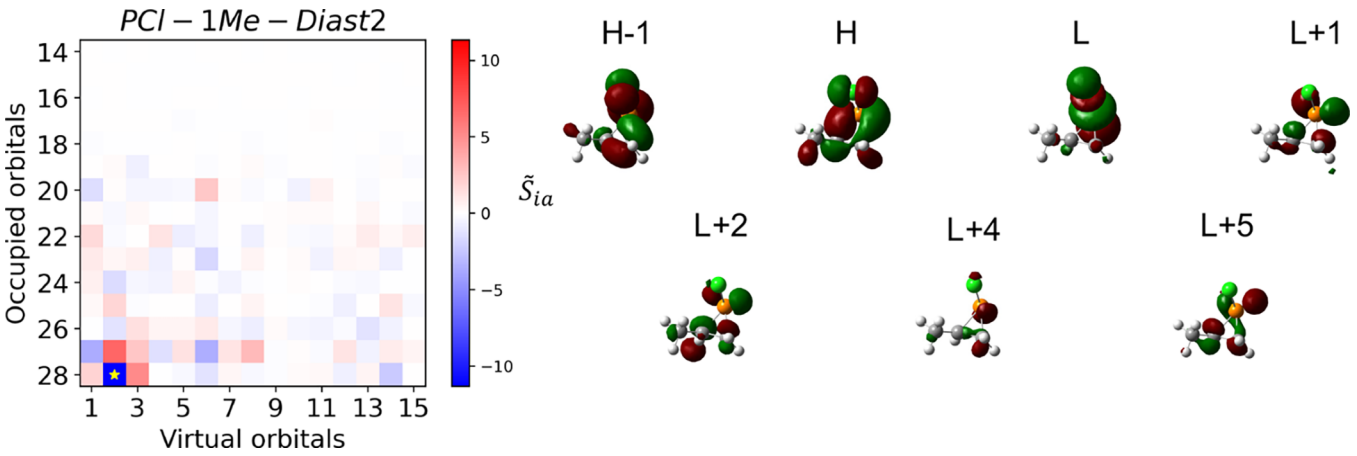

Figure 14. $\tilde{S}_{ia}$ of *PCl* − 1*Me* − *Diast*.2 at equilibrium geometry and visualizations of significant molecular orbitals. The ∗ denotes the largest transition.

https://doi.org/10.1021/acs.jpca.4c03728
J. Phys. Chem. A 2024, 128, 8045−8059

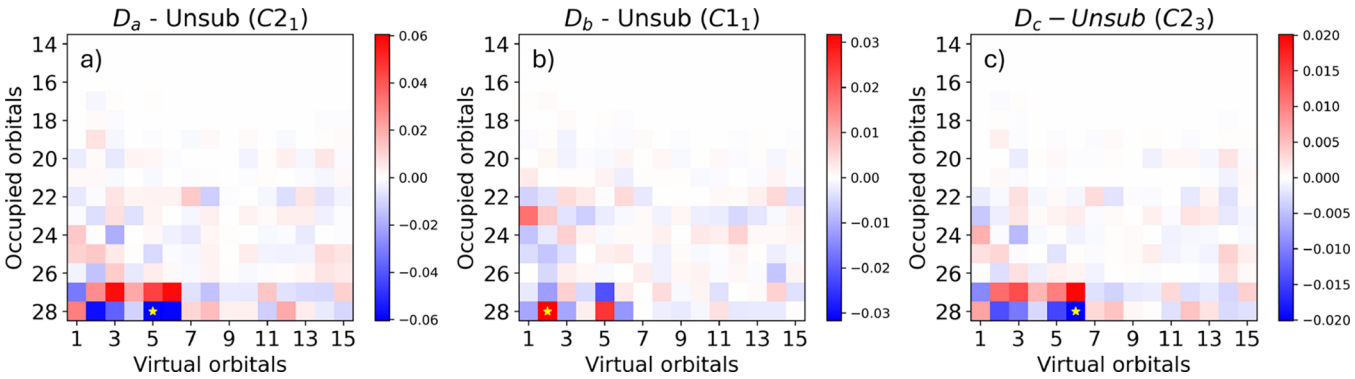

Figure 16. (a–c) $\Delta\Delta\tilde{S}_{ia}$ values normalized with respect to Tr($\boldsymbol{\beta}$) for *PCl* − 1*Me* − *Diast*.2 localized modes. The ∗ denotes the largest transition.

discussion of the $\Delta\Delta\ \tilde{S}_{ia}$ values. Also for this case, the $\Delta\tilde{S}_{ia}$ orbital analysis for selected normal and local modes is reported in the SI, Figures S14 and S15.

Three different local carbon stretching modes contribute greatly to each vibrational correction. $\Delta\Delta\tilde{S}_{ia}$ serves again as a metric of how the change in vibrational effects as a result of isotopic substitution affects the one-electron molecular orbital transitions. Figure 16a,c are qualitatively the same in terms of significant $\Delta\Delta\tilde{S}_{ia}$ values. However, while isotopic substitution has a similar effect on the $\tilde{S}_{ia}$ along these modes, the unsubstituted $\tilde{S}_{ia}$ along these modes has opposite sign, see Figure S15 in the SI. Thus, the same effect on the $\tilde{S}_{ia}$ is increasing the optical rotation upon substitution for one mode and decreasing it for the other. Localized mode $C2_1$ stretches along the direction of D_c's orientation whereas $C2_3$ stretches along the direction of D_a's orientation. It is reasonable that the largest $\Delta\Delta\tilde{S}_{ia}$ value for $C2_3$ are associated with the HOMO → LUMO+5 orbital transition, see Figure 14: in the LUMO+5 orbital the electron density is in part located over the D_a atom, corresponding to the direction of stretching of the mode. In Figure 15, the HOMO → LUMO+5 transition involves charge transfer toward the methyl group and a rotation of charge in the direction of H_a.

The $\Delta\Delta\tilde{S}_{ia}$ of the most important transitions can be decomposed into relative changes of the electric dipole and magnetic dipole density vector magnitudes as well as the change in the angle between the vectors. The values are normalized with respect to the corresponding quantity in the equilibrium transition. Table 2 shows the decomposition of the transitions HOMO → LUMO+1, LUMO+4, and LUMO+5. The HOMO → LUMO+4 transition for all three of the localized modes have significant changes in the electric dipole vector and the angle as a result of isotopic substitution. The HOMO → LUMO+5 also experiences a greater change in the electric dipole vector magnitude compared to the magnetic dipole density vector. The only outlier for these transitions is the HOMO → LUMO+1 transition that experiences the largest change in the magnetic dipole density vector. This vibration is for *C*1 bonded to the methyl group for a transition to a virtual orbital that still has π orbital character on the PCl moieties that is not seen in LUMO+4 and LUMO+5. Also for this molecule, the change in the cosine of the angle between the vectors is the largest contributor to the change in $\tilde{S}_{ia}$ for many of the transitions.

Table 2. Decomposition of $\Delta\Delta\tilde{S}_{ia}$ Values into % Change of Electric Dipole Vector Magnitude ($|\boldsymbol{\mu}|$), Magnetic Dipole Density Vector Magnitude ($|\boldsymbol{m}|$) and the cos($\boldsymbol{\theta}$) of the Vectors for Selected *PCl* − 1*Me* − *Diast*.2 Transitions[a]

localized mode	transition	$\Delta\Delta\lvert\mu\rvert$	$\Delta\Delta\lvert m\rvert$	$\Delta\Delta\cos(\theta)$
$C2_1$ (D_a)	HOMO → LUMO+4	7.11	−0.14	13.73
	HOMO → LUMO+5	0.61	0.25	4.12
$C1_1$ (D_b)	HOMO → LUMO+1	−0.02	−0.33	−0.03
	HOMO → LUMO+4	−5.20	−0.34	−3.25
$C2_3$ (D_c)	HOMO → LUMO+4	2.44	−0.25	7.69
	HOMO → LUMO+5	0.34	0.20	2.81

[a]All values are normalized with respect to the corresponding quantity at the equilibrium geometry and valid for a step size of 0.004. The isotope position for each vibrational mode is reported in parentheses.

5. DISCUSSION

In this work, we aim to study how the substitution of deuterium changes the overall optical rotation for a test set of chiral molecules. The isotope effect is quantified through the vibrational correction to the OR, expressed as the sum of $[\alpha]_{V1}$ and $[\alpha]_{V2}$, where the first term depends on the anharmonicity of the potential energy surface and the second term depends on the curvature of the property surface, see eq 3. The analysis is performed introducing Δ^{Rel} and $\Delta\Delta^{Rel}$, see eq 8, which normalize the vibrational correction of the unsubstituted and isotopically substituted molecules with respect to the equilibrium OR. The unsigned average $\Delta\Delta^{Rel}$ in Figure 2 shows that X groups with S and P moieties have the largest average change in vibrational correction magnitude. Thus, it appears that a polarizable heteroatom within the ring is important in producing a large isotope effect. On the other hand, polarizable heteroatoms in the Y position do not produce the same effect (for instance, compare the $\Delta\Delta^{Rel}$ value of NCl and PCl molecules in Figure 2). Focusing on the P and S moieties, Figure 3 shows that $[\alpha]_{V2}$ is the most important contribution to both the Δ^{Rel} and $\Delta\Delta^{Rel}$.

Figure 4 reports the Δ^{Rel} values of the unsubstituted molecule individually. One pattern observed is that the only cases of molecules having negative vibrational corrections of the unsubstituted molecule are when there is a fluorine and chlorine atom on the same side of the ring, such as *PCl* − 2*F* and *PCl* − 1*F* − *Diast*.2. Figure 6 shows that deuterium substitutions made to hydrogens bonded to the same carbon (D_a and D_c) always possess different $\Delta\Delta^{Rel}$ signs. For the unsubstituted molecule this carbon is not a stereocenter, but it becomes one after isotopic substitution. D_a and D_c substitution result in a stereocenter of differing Cahn-Ingold-Prelog designation corresponding to the handedness of the chiral

https://doi.org/10.1021/acs.jpca.4c03728
J. Phys. Chem. A 2024, 128, 8045−8059

center. Overall, it appears that for molecules with significant $\Delta\Delta^{Rel}$ values, the D_c isotopic substitution results in the largest magnitude optical rotation (as a reminder, we chose the enantiomers with positive $[\alpha]_{eq}$, thus positive Δ^{Rel} and $\Delta\Delta^{Rel}$ values correspond to an overall increase in the total OR, see eqs 2 and 8). Furthermore, Figure 7 shows that $\Delta\Delta^{Rel}$ is approximately additive for two deuterium substitutions. However, this can result in a doubly substituted molecule that has a total negative $[\alpha]_V$ though individual substitutions have positive $[\alpha]_V$ values, as shown in Figure 7b.

We chose four molecules with significant $\Delta\Delta^{Rel}$ values to analyze the vibrational contribution in terms of individual vibrations: $S-1F$, $S-1Me$, $PCl-1F-Diast.2$, and $PCl-1Me-Diast.2$. The vibrational corrections in terms of normal modes are reported in Figures S8 and S9 in the SI. There are many significant contributors to the sum, but we were not able to match the same modes across isotopologues because the isotopic substitution affects the energy and appearance of normal modes. Therefore, a localized vibrational basis was used for the analysis, which does not change the overall value of $[\alpha]_{V1}$ and $[\alpha]_{V2}$. Shown in Figures S10 and S11, the magnitude of $[\alpha]_{V1}$ and $[\alpha]_{V2}$ per mode is larger for the localized modes compared to the normal modes. Hydrogen wagging and stretching modes are significant contributors to the vibrational correction especially, for $[\alpha]_{V2}$. In addition, for $[\alpha]_{V1}$ of $PCl-1Me-Diast.2$ the carbon stretching vibrations are also significant contributors. The hydrogen wagging and stretching modes appear to be connected as the signs are the same for $[\alpha]_{V2}$ for all four of the molecules. Figures 9 and 10 indicate that wagging modes determine the overall sign of $\Delta\Delta^{Rel}$ for that isotopic substitution. For example, $PCl-1F-Diast.2$ has negative vibrational correction values for the D_a and D_b wagging modes and an overall positive $\Delta\Delta^{Rel}$. The other three molecules have opposite signs for these hydrogen wagging modes and as a result, negative $\Delta\Delta^{Rel}$ values for D_a and D_b. For $S-1F$, the localized mode with the largest $\Delta\Delta^{Rel}$ that matches the sign of the sum is the hydrogen wagging for all three of the isotopologues. Considering $S-1Me$ and $PCl-1F-Diast.2$, for two of the three isotopologues hydrogen wagging is the most important contributor to the change in the vibrational correction. It is only $PCl-1Me-Diast.2$ that deviates from this pattern, as carbon stretching modes are the most significant contributor to the $\Delta\Delta^{Rel}$. It is somewhat surprising that the effect on the vibrational correction for deuterium stretching is relatively small compared to other localized modes, especially wagging modes, see Figures 9 and 10. As discussed more in detail below, the relatively small $\Delta\Delta^{Rel}$ effect of the stretching modes involving the deuterium atoms compared to their wagging modes is due to the truly localized nature of the former modes: stretching after isotopic substitution does not affect the electron density surrounding the polarizable atoms because the molecular frame is virtually not moving for these modes, and there is little electron density localized around the H/D center itself; on the other hand, H/D wagging alters the molecular frame structure and the difference in mass between isotopes is sufficient to affect the electron density response during the vibrational motion.

The $\tilde{S}_{ia}$ analysis, performed for $PCl-1F-Diast.2$ and $PCl-1Me-Diast.2$, examines how isotopic substitution affects the MO transitions responsible for changes in the vibrational correction for two different R groups. These molecules were chosen due to their significant $\Delta\Delta^{Rel}$ values for their localized modes presented in Figures 9 and 10. For $PCl-1F-Diast.2$ normal and localized modes, the largest $\Delta\tilde{S}_{ia}$ values are for the HOMO−1 and HOMO → LUMO and LUMO+1, which correspond to transitions that are already significant at equilibrium (compare Figures 11 and S13 in the SI). The HOMO → LUMO transition, visualized in Figure 12, features prominent rotation of charge in the direction of the PCl group. The transitions to the LUMO+1 feature prominent linear flow of charge between the chlorine and fluorine atoms for the HOMO−1 orbital and toward the phosphorus atom for the HOMO. For the localized modes, we can examine how the isotopic substitution affects the electronic processes associated with the vibrations through $\Delta\Delta\tilde{S}_{ia}$, see eq 9. Figure 13 presents the $\Delta\Delta\tilde{S}_{ia}$ values for four hydrogen wagging modes and one carbon stretching mode. The largest $\Delta\Delta\tilde{S}_{ia}$ values are associated with the HOMO → LUMO transition for three of the four hydrogen wagging modes. The outlier of the hydrogen wagging modes, D_b1, possesses the greatest $\Delta\Delta\tilde{S}_{ia}$ value for the HOMO−1 → LUMO+1 transition, which features significant rotation and linear flow of charge between the PCl group and fluorine atom. Isotopic substitution affects the trajectory of the carbon stretching mode, which in turn affects the linear flow of charge to the phosphorus atom. The decomposition of the $\Delta\Delta\tilde{S}_{ia}$ values into the differences in the dot product components, reported in Table 1, shows that the largest difference for the electric dipole vector occurs for modes D_a1 and D_b1, whereas the largest difference for the magnetic dipole density vector magnitude occurs for D_a2, H_b2, and $C1_2$. Both of the D_a modes lead to an increase in the electric dipole vector magnitudes as a result of isotopic substitution, whereas this value decreases for D_b modes. For $PCl-1Me-Diast.2$, the primary difference of the $\Delta\Delta\tilde{S}_{ia}$ analysis compared to $PCl-1F-Diast.2$ is the inclusion of transitions involving the LUMO+4 and LUMO+5 orbitals, which were not significant at equilibrium. These transitions involve significant changes in the angle between the vectors ($\Delta\Delta\cos(\theta)$) for LUMO+4 and due to the changes in the electric dipole vector for LUMO+5 ($\Delta\Delta|\boldsymbol{\mu}|$), shown in Table 2. The inclusion of the methyl group of the molecule results in changes of these molecular orbital transitions for the carbon stretching modes that are not seen for when the R group is a fluorine atom.

Therefore, isotopic substitution has a significant effect for vibrations that alter the MO transitions that are already important at equilibrium, i.e., the most important contributors to $[\alpha]_{eq}$. In general, these transitions involve circular flow of charge around the ring, linear flow of charge from the ring to Y atom, or linear flow of charge from the R group to the X moiety. Although we have not investigated all molecules at this level of detail, it is likely that these types of transitions are important for all X moieties and all R groups. However, only polarizable X groups have electron density that is diffuse enough to feel the subtle effect of change of mass due to isotopic substitution. In particular, this change of mass is most effective in affecting the OR for modes that change the ring frame of the molecules, i.e., H/D wagging modes, or when the H/D is bonded to a vibrating C center.

6. CONCLUSIONS

In this work, we systematically examine the effect of isotopic substitution on the optical rotation on a test set of small chiral organic molecules of similar structure: three-member rings with an heteroatom in the ring and one or two electron-directing substituent groups bonded to carbon atoms in the

https://doi.org/10.1021/acs.jpca.4c03728
J. Phys. Chem. A 2024, 128, 8045−8059

ring, see Figure 1. We consider H → D isotopic substitutions of each H atom bonded to the ring carbons (substitutions on the ligands provided small effects and were not considered further). Here, we summarize the key outcomes of the study.

First, the isotopic substitution has the largest effect for molecules with polarizable heteroatoms in the ring, i.e., those with S, PH, and PCl. For these groups, the $[\alpha]_{V2}$ term (see eq 3) is the largest contributor to both the absolute vibrational correction and the change in the vibrational correction due to isotopic substitution, see Figure 3. In most cases, see Figure 6, the location of isotopic substitution that results in the largest total optical rotation is D_c (i.e., when the change in $[\alpha]_V$ has the same sign as $[\alpha]_{eq}$, see eq 2). However, for X = PCl and the R = F atom on the same side of the ring as the chlorine, the unsubstituted molecule has a negative $[\alpha]_V$. Thus, although the D_c substitution has a large effect, in this case it is opposite in sign to $[\alpha]_{eq}$ and it reduces the overall OR magnitude (this is the same argument for D_a and D_b substitutions, which have large effects but in the wrong direction, see Figure 6). Therefore, for this molecule the isotopic substitution that results in the largest OR is D_b. Typically, molecules with one R group experience a larger isotopic effect than those with two R groups, probably because of the larger relative change in reduced mass of vibrational modes.

A more detailed analysis of individual vibrational modes contributions was conducted on the molecules with the largest isotopic effect (i.e., *S − 1F*, *S − 1Me*, *PCl − 1F − Diast.2*, and *PCl − 1Me − Diast.2*). This analysis uses localized vibrational modes rather than normal modes, because the latter change significantly in nature due to isotopic substitution and are not easily comparable across isotopologues. The hydrogen stretching and wagging modes are significant contributors to the vibrational correction and, in addition, the carbon stretching modes for *PCl − 1Me − Diast.2*, see Figures S10 and S11 in the SI. However, the largest isotopic effect occurs for H wagging modes for most molecules rather than for stretching modes, as shown in Figures 9 and 10. For some cases, like the *PCl − 1Me − Diast.2* molecule, carbon stretching modes also induce large isotopic effects.

These observations are rationalized considering how isotopic substitution changes the effect of the most significant vibrational modes on the most important electronic transitions between molecular orbitals, using the $\tilde{S}_{ia}$ analysis. Specifically, isotopic substitution affects the same four or five main transitions that determine the overall sign of the equilibrium OR ($[\alpha]_{eq}$), e.g., compare Figures 11 and 13 for molecule *PCl − 1F − Diast.2*. These significant transitions involve circular flow of charge around the ring, linear flow of charge from the ring to Y atom, or linear flow of charge from the R group to the X moiety. Although these transitions are probably present for all X groups, it is only with the most polarizable ones that the isotopic effect becomes noticeable, because the electron density surrounding these groups can be more easily displaced. Furthermore, H/D wagging modes are those where the effect on the molecular frame is most sensitive to the change in mass due to isotopic substitution, thus affecting the fine balance between electric and magnetic dipole moments (i.e., their magnitude and especially their relative orientation, see Table 1), with significant effects on the overall OR. This is in contrast with H/D stretching modes, where the change in the vibration is localized and it affects only the small amount of electron density around the H/D center. Molecule *PCl − 1Me − Diast.2* also shows that isotopic substitution can affect localized modes of the C atoms directly attached to the H/D center, with effects similar to those of the H/D wagging vibrations (see Table 2). In this case, these transitions become relevant only after isotopic substitution.

In summary, this work provides insights into the isotope effect on optical rotation, in terms of relevant vibrational motion and electronic charge flow. It would be interesting to see whether these predictions will be confirmed by experimental measurements. In the future, we will apply these insights to study whether achiral molecules can be imbued with a significant optical activity via isotopic substitution and whether this may affect their chemical properties.

■ ASSOCIATED CONTENT

Supporting Information

The Supporting Information is available free of charge at https://pubs.acs.org/doi/10.1021/acs.jpca.4c03728.

Optimized geometries for all test molecules included separately as xyz files (ZIP)

Explicit structure, name, and numbering of all 50 molecules, Figures S1−S7; calculated values of $[\alpha]_{eq}$, $[\alpha]_{V1}$, and $[\alpha]_{V2}$ for all test molecules and isotopic substitutions, Tables S1−S7; corresponding individual normal mode contributions, Tables S8−S23; localized mode contributions, Tables S24−S31; $[\alpha]_{V1}$ and $[\alpha]_{V2}$ normal mode plots for each isotopologue of molecules *S − 1F*, *PCl − 1F − Diast.2*, *S − 1Me* and *PCl − 1Me − Diast.2*, Figures S8 and S9, including a discussion of the data; $[\alpha]_{V1}$ and $[\alpha]_{V2}$ localized mode plots for each isotopologue of the same four molecules, Figures S10 and S11, including a discussion of the data; $\Delta\tilde{S}_{ia}$ heatmap plots for selected normal modes of *PCl − 1F − Diast.2* along with visualizations of displacement vectors, Figure S12, including a discussion of the data; $\Delta\tilde{S}_{ia}$ heatmap plots for selected localized modes of *PCl − 1F − Diast.2*, Figure S13, including a discussion of the data; $\Delta\tilde{S}_{ia}$ heatmap plots for selected normal modes of *PCl − 1Me − Diast.2* along with visualizations of displacement vectors, Figure S14, including a discussion of the data; and $\Delta\tilde{S}_{ia}$ heatmap plots for selected localized modes of *PCl − 1Me − Diast.2*, Figure S15, including a discussion of the data (PDF)

■ AUTHOR INFORMATION

Corresponding Author

Marco Caricato − *Department of Chemistry, University of Kansas, Lawrence, Kansas 66045, United States;* orcid.org/0000-0001-7830-0562; Email: mcaricato@ku.edu

Authors

Brian Faintich − *Department of Chemistry, University of Kansas, Lawrence, Kansas 66045, United States*

Taylor Parsons − *Department of Chemistry, University of Kansas, Lawrence, Kansas 66045, United States*

Ty Balduf − *Department of Chemistry, University of Kansas, Lawrence, Kansas 66045, United States;* orcid.org/0000-0002-2066-2314

Complete contact information is available at: https://pubs.acs.org/10.1021/acs.jpca.4c03728

Notes

The authors declare no competing financial interest.

■ ACKNOWLEDGMENTS

The authors gratefully acknowledge support from the National Science Foundation through Grant No. CHE-2154452. The calculations were performed at the University of Kansas Center for Research Computing (CRC), including the BigJay cluster resource funded through NSF Grant MRI-2117449.

■ REFERENCES

(1) Cahn, R. S.; Ingold, C.; Prelog, V. Specification of Molecular Chirality. *Angew. Chem., Int. Ed. Engl.* **1966**, *5*, 385−415.
(2) Barron, L. D. *Molecular Light Scattering and Optical Activity*; Cambridge University Press, 2004.
(3) Wnendt, S.; Zwingenberger, K. Thalidomide's chirality. *Nature* **1997**, *385*, 303−304.
(4) Brooks, W. H.; Guida, W. C.; Daniel, K. G. The significance of chirality in drug design and development. *Curr. Top. Med. Chem.* **2011**, *11*, 760−770.
(5) Coelho, M. M.; Fernandes, C.; Remião, F.; Tiritan, M. E. Enantioselectivity in Drug Pharmacokinetics and Toxicity: Pharmacological Relevance and Analytical Methods. *Molecules* **2021**, *26*, 3113.
(6) Cymerman Craig, J.; Roy, S. K. Optical rotatory dispersion and absolute configuration—I: α-Amino acids. *Tetrahedron* **1965**, *21*, 391−394.
(7) Gaffield, W. Circular dichroism, optical rotatory dispersion and absolute configuration of flavanones, 3-hydroxyflavanones and their glycosides: Determination of aglycone chirality in flavanone glycosides. *Tetrahedron* **1970**, *26*, 4093−4108.
(8) Berova, N.; Bari, L. D.; Pescitelli, G. Application of electronic circular dichroism in configurational and conformational analysis of organic compounds. *Chem. Soc. Rev.* **2007**, *36*, 914−931.
(9) Polavarapu, P. L. Optical rotation: Recent advances in determining the absolute configuration. *Chirality* **2002**, *14*, 768−781.
(10) Wiberg, K. B.; Vaccaro, P. H.; Cheeseman, J. R. Conformational Effects on Optical Rotation. 3-Substituted 1-Butenes. *J. Am. Chem. Soc.* **2003**, *125*, 1888−1896.
(11) Autschbach, J. Computing chiroptical properties with first-principles theoretical methods: Background and illustrative examples. *Chirality* **2009**, *21*, E116−E152.
(12) Crawford, T. D.; Tam, M. C.; Abrams, M. L. The Current State of Ab Initio Calculations of Optical Rotation and Electronic Circular Dichroism Spectra. *J. Phys. Chem. A* **2007**, *111*, 12057−12068.
(13) Stephens, P. J.; Devlin, F. J.; Cheeseman, J. R.; Frisch, M. J. Calculation of Optical Rotation Using Density Functional Theory. *J. Phys. Chem. A* **2001**, *105*, 5356−5371.
(14) Cheeseman, J. R.; Frisch, M. J.; Devlin, F. J.; Stephens, P. J. Hartree-Fock and Density Functional Theory ab Initio Calculation of Optical Rotation Using GIAOs: Basis Set Dependence. *J. Phys. Chem. A* **2000**, *104*, 1039−1046.
(15) Stephens, P. J.; McCann, D. M.; Cheeseman, J. R.; Frisch, M. J. Determination of absolute configurations of chiral molecules using ab initio time-dependent Density Functional Theory calculations of optical rotation: how reliable are absolute configurations obtained for molecules with small rotations? *Chirality* **2005**, *17*, S52−64.
(16) Ruud, K.; Helgaker, T. Optical rotation studied by density-functional and coupled-cluster methods. *Chem. Phys. Lett.* **2002**, *352*, 533−539.
(17) Autschbach, J.; Patchkovskii, S.; Ziegler, T.; van Gisbergen, S. J. A.; Jan Baerends, E. Chiroptical properties from time-dependent density functional theory. II. Optical rotations of small to medium sized organic molecules. *J. Chem. Phys.* **2002**, *117*, 581−592.
(18) Krykunov, M.; Autschbach, J. Calculation of optical rotation with time-periodic magnetic-field-dependent basis functions in approximate time-dependent density-functional theory. *J. Chem. Phys.* **2005**, *123*, No. 114103.
(19) Zuber, G.; Goldsmith, M.-R.; Beratan, D. N.; Wipf, P. Assignment of the absolute configuration of [n]-ladderanes by TD-DFT optical rotation calculations. *Chirality* **2005**, *17*, 507−510.
(20) Grimme, S. Calculation of frequency dependent optical rotation using density functional response theory. *Chem. Phys. Lett.* **2001**, *339*, 380−388.
(21) Crawford, T. D.; Owens, L. S.; Tam, M. C.; Schreiner, P. R.; Koch, H. Ab Initio Calculation of Optical Rotation in (P)-(+)-[4]Triangulane. *J. Am. Chem. Soc.* **2005**, *127*, 1368−1369.
(22) McCann, D. M.; Stephens, P. J. Determination of Absolute Configuration Using Density Functional Theory Calculations of Optical Rotation and Electronic Circular Dichroism: Chiral Alkenes. *J. Org. Chem.* **2006**, *71*, 6074−6098.
(23) Pecul, M.; Ruud, K.; Rizzo, A.; Helgaker, T. Conformational Effects on the Optical Rotation of Alanine and Proline. *J. Phys. Chem. A* **2004**, *108*, 4269−4276.
(24) Crawford, T. D.; Stephens, P. J. Comparison of Time-Dependent Density-Functional Theory and Coupled Cluster Theory for the Calculation of the Optical Rotations of Chiral Molecules. *J. Phys. Chem. A* **2008**, *112*, 1339−1345.
(25) McCann, D. M.; Stephens, P. J.; Cheeseman, J. R. Determination of Absolute Configuration Using Density Functional Theory Calculation of Optical Rotation: Chiral Alkanes. *J. Org. Chem.* **2004**, *69*, 8709−8717.
(26) Wiberg, K. B. The Deuterium Isotope Effect. *Chem. Rev.* **1955**, *55*, 713−743.
(27) Verbit, L. *Progress in Physical Organic Chemistry*; John Wiley & Sons, Ltd, 1970; pp 51−127.
(28) Holzwarth, G.; Chabay, I. Optical Activity of Vibrational Transitions: A Coupled Oscillator Model. *J. Chem. Phys.* **1972**, *57*, 1632−1635.
(29) Dezentje, R. F. R.; Dekkers, H. P. J. M. Calculations on the optical activity due to isotopic substitution: [1-D]- and [2−18O]-α-fenchocamphoronequinone. Relationship to the optical activity of 1-substituted α-diones. *Chem. Phys.* **1976**, *18*, 189−197.
(30) Barth, G.; Djerassi, C. Circular dichroism of molecules with isotopically engendered chirality. *Tetrahedron* **1981**, *37*, 4123−4142.
(31) Polavarapu, P. L.; Nafie, L. A.; Benner, S. A.; Morton, T. H. Optical activity due to isotopic substitution. Vibrational circular dichroism and the absolute configurations of.alpha.-deuterated cyclohexanones. *J. Am. Chem. Soc.* **1981**, *103*, 5349−5354. Publisher: American Chemical Society.
(32) Dierksen, M.; Grimme, S. A theoretical study of the chiroptical properties of molecules with isotopically engendered chirality. *J. Chem. Phys.* **2006**, *124*, No. 174301.
(33) Cohan, N. V.; Hameka, H. F. Isotope Effects in Optical Rotation1. *J. Am. Chem. Soc.* **1966**, *88*, 2136−2142. Publisher: American Chemical Society.
(34) Green, M. M.; Andreola, C.; Munoz, B.; Reidy, M. P.; Zero, K. Macromolecular stereochemistry: a cooperative deuterium isotope effect leading to a large optical rotation. *J. Am. Chem. Soc.* **1988**, *110*, 4063−4065.
(35) Cantekin, S.; Balkenende, D. W. R.; Smulders, M. M. J.; Palmans, A. R. A.; Meijer, E. W. The effect of isotopic substitution on the chirality of a self-assembled helix. *Nat. Chem.* **2011**, *3*, 42−46. Publisher: Nature Publishing Group.
(36) Ruden, T. A.; Lutnæs, O. B.; Helgaker, T.; Ruud, K. Vibrational corrections to indirect nuclear spin−spin coupling constants calculated by density-functional theory. *J. Chem. Phys.* **2003**, *118*, 9572−9581.
(37) Ruud, K.; Åstrand, P.-O.; Taylor, P. R. Zero-Point Vibrational Effects on Proton Shieldings: Functional-Group Contributions from ab Initio Calculations. *J. Am. Chem. Soc.* **2001**, *123*, 4826−4833.
(38) Pfeiffer, F.; Rauhut, G.; Feller, D.; Peterson, K. A. Anharmonic zero point vibrational energies: Tipping the scales in accurate thermochemistry calculations? *J. Chem. Phys.* **2013**, *138*, No. 044311.
(39) Grev, R. S.; Janssen, C. L.; Schaefer, H. F. III Concerning zero-point vibrational energy corrections to electronic energies. *J. Chem. Phys.* **1991**, *95*, 5128−5132.

https://doi.org/10.1021/acs.jpca.4c03728
J. Phys. Chem. A 2024, 128, 8045−8059

(40) Kern, C. W.; Matcha, R. L. Nuclear Corrections to Electronic Expectation Values: Zero-Point Vibrational Effects in the Water Molecule. *J. Chem. Phys.* **1968**, *49*, 2081−2091.
(41) Krohn, B. J.; Ermler, W. C.; Kern, C. W. Nuclear corrections to molecular properties. IV. Theory for low-lying vibrational states of polyatomic molecules with application to the water molecule near the Hartree-Fock limit. *J. Chem. Phys.* **1974**, *60*, 22−33.
(42) Ermler, W. C.; Kern, C. W. Zero-Point Vibrational Corrections to One-Electron Properties of the Water Molecule in the Near-Hartree-Fock Limit. *J. Chem. Phys.* **1971**, *55*, 4851−4860.
(43) Åstrand, P.-O.; Ruud, K.; Sundholm, D. A modified variation−perturbation approach to zero-point vibrational motion. *Theor. Chem. Acc.* **2000**, *103*, 365−373.
(44) Bishop, D. M.; Kirtman, B. A perturbation method for calculating vibrational dynamic dipole polarizabilities and hyperpolarizabilities. *J. Chem. Phys.* **1991**, *95*, 2646−2658.
(45) Eckart, U.; Ingamells, V. E.; Papadopoulos, M. G.; Sadlej, A. J. Vibrational effects on electric properties of cyclopropenone and cyclopropenethione. *J. Chem. Phys.* **2001**, *114*, 735−745.
(46) Avramopoulos, A.; Ingamells, V. E.; Papadopoulos, M. G.; Sadlej, A. J. Vibrational corrections to electric properties of relativistic molecules: The coinage metal hydrides. *J. Chem. Phys.* **2001**, *114*, 198−210.
(47) Aharon, T.; Lemler, P.; Vaccaro, P. H.; Caricato, M. Comparison of measured and predicted specific optical rotation in gas and solution phases: A test for the polarizable continuum model of solvation. *Chirality* **2018**, *30*, 383−395.
(48) Mort, B. C.; Autschbach, J. Magnitude of Zero-Point Vibrational Corrections to Optical Rotation in Rigid Organic Molecules: A Time-Dependent Density Functional Study. *J. Phys. Chem. A* **2005**, *109*, 8617−8623.
(49) Ruud, K.; Taylor, P. R.; Åstrand, P.-O. Zero-point vibrational effects on optical rotation. *Chem. Phys. Lett.* **2001**, *337*, 217−223.
(50) Caricato, M. Orbital Analysis of Molecular Optical Activity Based on Configuration Rotatory Strength. *J. Chem. Theory Comput.* **2015**, *11*, 1349−1353.
(51) Caricato, M. Conformational Effects on Specific Rotation: A Theoretical Study Based on the S_k Method. *J. Phys. Chem. A* **2015**, *119*, 8303−8310.
(52) Aharon, T.; Caricato, M. Configuration Space Analysis of the Specific Rotation of Helicenes. *J. Phys. Chem. A* **2019**, *123*, 4406−4418.
(53) Balduf, T.; Caricato, M. Gauge Dependence of the S_k Molecular Orbital Space Decomposition of Optical Rotation. *J. Phys. Chem. A* **2021**, *125*, 4976−4985.
(54) Balduf, T.; Caricato, M. Origin invariant molecular orbital decomposition of optical rotation. *Theor. Chem. Acc.* **2023**, *142*, 11.
(55) Buckingham, A. D.; Dunn, M. B. Optical activity of oriented molecules. *J. Chem. Soc. A* **1971**, 1988−1991.
(56) Crawford, T. D. Ab initio calculation of molecular chiroptical properties. *Theor. Chem. Acc.* **2006**, *115*, 227−245.
(57) Pipek, J.; Mezey, P. G. A fast intrinsic localization procedure applicable for ab initio and semiempirical linear combination of atomic orbital wave functions. *J. Chem. Phys.* **1989**, *90*, 4916−4926.
(58) Jacob, C. R.; Reiher, M. Localizing normal modes in large molecules. *J. Chem. Phys.* **2009**, *130*, No. 084106.
(59) Becke, A. D. Density-functional thermochemistry. III. The role of exact exchange. *J. Chem. Phys.* **1993**, *98*, 5648−5652.
(60) Dunning, T. H., Jr. Gaussian basis sets for use in correlated molecular calculations. I. The atoms boron through neon and hydrogen. *J. Chem. Phys.* **1989**, *90*, 1007−1023.
(61) Frisch, M. J.; Trucks, G. W.; Schlegel, H. B.; Scuseria, G. E.; Robb, M. A.; Cheeseman, J. R.; Scalmani, G.; Barone, V.; Petersson, G. A.; Nakatsuji, H. et al. *Gaussian Development Version Revision J.11.*; Gaussian, Inc., **2018**.
(62) Schrödinger, LLC. *The PyMOL Molecular Graphics System, Version 2.5.0.*; Schrödinger, LLC, 2018.
(63) Barclay, M. S.; Quincy, T. J.; Williams-Young, D. B.; Caricato, M.; Elles, C. G. Accurate Assignments of Excited-State Resonance Raman Spectra: A Benchmark Study Combining Experiment and Theory. *J. Phys. Chem. A* **2017**, *121*, 7937−7946.
(64) Tao, Y.; Zou, W.; Nanayakkara, S.; Kraka, E. PyVibMS: a PyMOL plugin for visualizing vibrations in molecules and solids. *J. Mol. Model.* **2020**, *26*, 290.

https://doi.org/10.1021/acs.jpca.4c03728
J. Phys. Chem. A 2024, 128, 8045−8059